Photo-physiological Acclimation in *Synechocystis* sp. PCC 6803 Provides Insight into Growth Limitation in Underwater Spectra

Tomáš Zavřel[1*], Anna Segečová[1], László Kovács[2], Martin Lukeš[3], Zoltán Novák[4], Milán Szabó[2], Boglárka Somogyi[4], Ondřej Prášil[3], Jan Červený[1], Gábor Bernát[4*]

[1]Global Change Research Institute of the Czech Academy of Sciences, Brno, 603 00, Czechia

[2]Biological Research Centre, Eötvös Loránd Research Network (ELKH), Szeged, 6726, Hungary

[3]Centre Algatech, Institute of Microbiology of the Czech Academy of Sciences, Třeboň, 379 01, Czechia

[4]Balaton Limnological Research Institute, Eötvös Loránd Research Network (ELKH), Tihany, 8237, Hungary

[*]email: zavrel.t@czechglobe.cz; bernat.gabor@blki.hu

Abstract

Cyanobacteria, as a substantial part of phytoplankton, play a key role in primary production in oceans and fresh waters. During their life, cyanobacteria cells needs to acclimate to a multitude of challenges, including shifts in a quality of underwater spectra. Recent progress in large scale environmental sampling and computational modelling provided insight into the effect of light spectrum on geographical distribution of cyanobacteria. However, detailed understanding to fitness advantage and limitations in the context of light quality has been missing. Here, we study photo-physiological acclimation in cyanobacterium *Synechocystis* sp. PCC 6803 through the whole range of photosynthetically active radiation (PAR). Using LEDs with qualitatively different narrow spectra, we describe wavelength dependency of light capture, electron transport rates and energy transduction to biomass, including fine-tuning processes such as state transitions and phycobilisomes attachment to photosystems. We show that growth was the most limited under blue light, due to extremely inefficient light harvesting. Even a low intensity of blue light induced PQ pool reduction and lead to the accumulation of reactive oxygen species. The PSI to PSII ratio was low under blue light, however, it was not the main limiting factor, since it was even more reduced under violet and near-far-red lights, where *Synechocystis* grew faster compared to blue light. Our results provide insight into the spectral dependency of growth in natural environments, and can provide a lead for light optimization in controlled cultivations.

Keywords

Light harvesting, Light quality, Photosynthesis, Photomorphogenesis, State transitions, Synechocystis

Introduction

Primary production in oceans and freshwaters relies on the ability of phytoplankton to acclimate to the ever-changing environmental conditions. The factors that determine abundance of phytoplankton in natural waters include temperature, nutrients, pH, and both intensity and quality of the incident light. Among these, the impact of light quality, i.e. a specific characteristic of the underwater spectra, has been for long the least studied phenomenon. However, as evident from the recent studies, the underwater spectrum is one of the essential factors that drive worldwide phytoplankton distribution (Grébert et al., 2018; Holtrop et al., 2021). The underwater spectra differ in eutrophic, mesotrophic or eutrophic waters. In clear waters, where only water molecules absorb and scatter light, green or blue photons become dominant with the increasing depth of the water column. On the contrary, the presence of organic matter shifts the light spectrum towards red wavelengths (Kirk, 2011).

Microalgae and cyanobacteria have developed numerous mechanisms to optimize light harvesting and energy transduction in the conditions of either excessive or limited light availability. In cyanobacteria, the short-term light acclimation processes include state transitions (ST) (Calzadilla and Kirilovsky, 2020), decoupling of light-harvesting antenna (Tamary et al., 2012), non-photochemical quenching (NPQ) (Kirilovsky and Kerfeld, 2016), heat dissipation (Demmig-Adams and Adams, 2006), activation of futile cycles such as cycling of inorganic carbon between cells and the environment (Müller et al., 2019; Tchernov et al., 2003), scavenging of reactive oxygen species (Pospíšil, 2012), or shifts in transcriptome (Luimstra et al., 2020). The long-term acclimation involves complex changes in proteome (Zavřel et al., 2019) including ratio of photosystem I (PSI) to photosystem II (PSII) (Luimstra et al., 2020), regulation of synthesis of energy-buffering molecules such as glycogen (Cano et al., 2018) or lipids (Zavřel et al., 2018c) and modifications of photosynthetic antenna within chromatic acclimation (CA). The latter process provides a great advantage in spectrally-limited underwater conditions; while many strains are restricted only to certain spectral niches, the chromatic acclimators can efficiently utilize broader spectrum of available light and therefore significantly increase the area and depth of suitable habitats (Sanfilippo et al., 2019).

While the molecular mechanisms of rearrangement of the light harvesting antenna during CA are known to a great detail (Grébert et al., 2021; Sanfilippo et al., 2019),

much less attention has been paid to the implications of underwater spectra shift on phytoplankton energetics and metabolism. The summary of metabolic changes as a response to light signals is called photomorphogenesis (Bernát et al., 2021; Montgomery, 2016), or photoacclimation. Even though response to individual wavelengths has been studied to some extent for chromatic acclimators (Kumar et al., 2018; Montgomery, 2016) as well as for strains not capable of CA (Luimstra et al., 2020; Singh et al., 2009), only a few studies provided a complex understanding to cellular energetics under light quality shift (Bernát et al., 2021). This is surprising, since the light quality-dependent plasticity of phytoplankton metabolism ultimately determines its abundance in the environment (Holtrop et al., 2021).

This study provides a detailed report on light quality acclimation in cyanobacterium *Synechocystis* sp. PCC 6803 (hereafter referred as *Synechocystis*). *Synechocystis* is a type 1 chromatic acclimator (CA1). It has a specific i) green light-dependent redistribution of light energy between photosystems through the linker CpcL that binds phycobilisomes (PBS) preferentially to photosystem I (PSI), and ii) a red light-dependent binding of the phycocyanin rods (PC) to allophycocyanin core (APC) through CpcG1 linker that helps to form canonical PBS (for more details see review (Sanfilippo et al., 2019)). The red/green light photoreceptor CcaS is common for chromatic acclimators of type 1-3 (CA1-3) (Wang and Chen, 2022), whereas the CpcL linker is present in many strains that are even not classified as chromatic acclimators (Hirose et al., 2019). The light acclimation in *Synechocystis* thus partially reveals photoacclimation strategies of other phytoplankton species that do not possess CA2-6 (Sanfilippo et al., 2019). One example is a close *Synechocystis* relative *Cyanobium gracile* that adopted both common and unique photoacclimation traits (Bernát et al., 2021).

Results of this study provide insight into spectral limitations of CA1 cyanobacteria in the environment, by addressing light capture and energy transduction efficiency in the context of availability of individual parts of the light spectrum. The cutivation setup, covering the whole range of visible light spectrum, reveals wavelength dependency of cell composition and photosynthesis efficiency between and outside of the most and the least suitable wavelengths for *Synechocystis* growth (red and blue photons, respectively). The results extend our understanding to phytoplankton limitation in natural environments, and can shape design of new strains as well as cultivation strategies of cyanobacteria in the production systems.

Results

Growth rate is tightly linked with the rate of electron flow

For the experiments, light intensity of nine monochromatic LEDs was set to 25 µmol photons m^{-2} s^{-1} (*Fig. 1a*). *Synechocystis* was growing with the highest specific growth rate under red LEDs, with peak wavelengths of 596 – 663 nm (*Fig. 1b*). This was surprising, since the photosynthetically usable radiation (PUR, *Fig. 1*a) as calculated from photosynthetically active radiation (PAR) and absorption spectra, was the highest under violet and blue light and the lowest under red light (*Fig. 1a*). High growth rates were accompanied by high linear electron flow from PSII to PSI (LEF), cyclic electron flow around PSI (PSI-CEF) and respiratory electron flow (REF), that were all upregulated under red light and downregulated under blue light (*Fig. 1c*). Electron flow through PSI was limited on the donor side under blue, green, yellow and orange light (peak wavelengths: 465 – 596 nm). PSI limitation on the acceptor side was not wavelength-dependent, despite it was slightly increased under 687 nm LED (*Fig. 1d*).

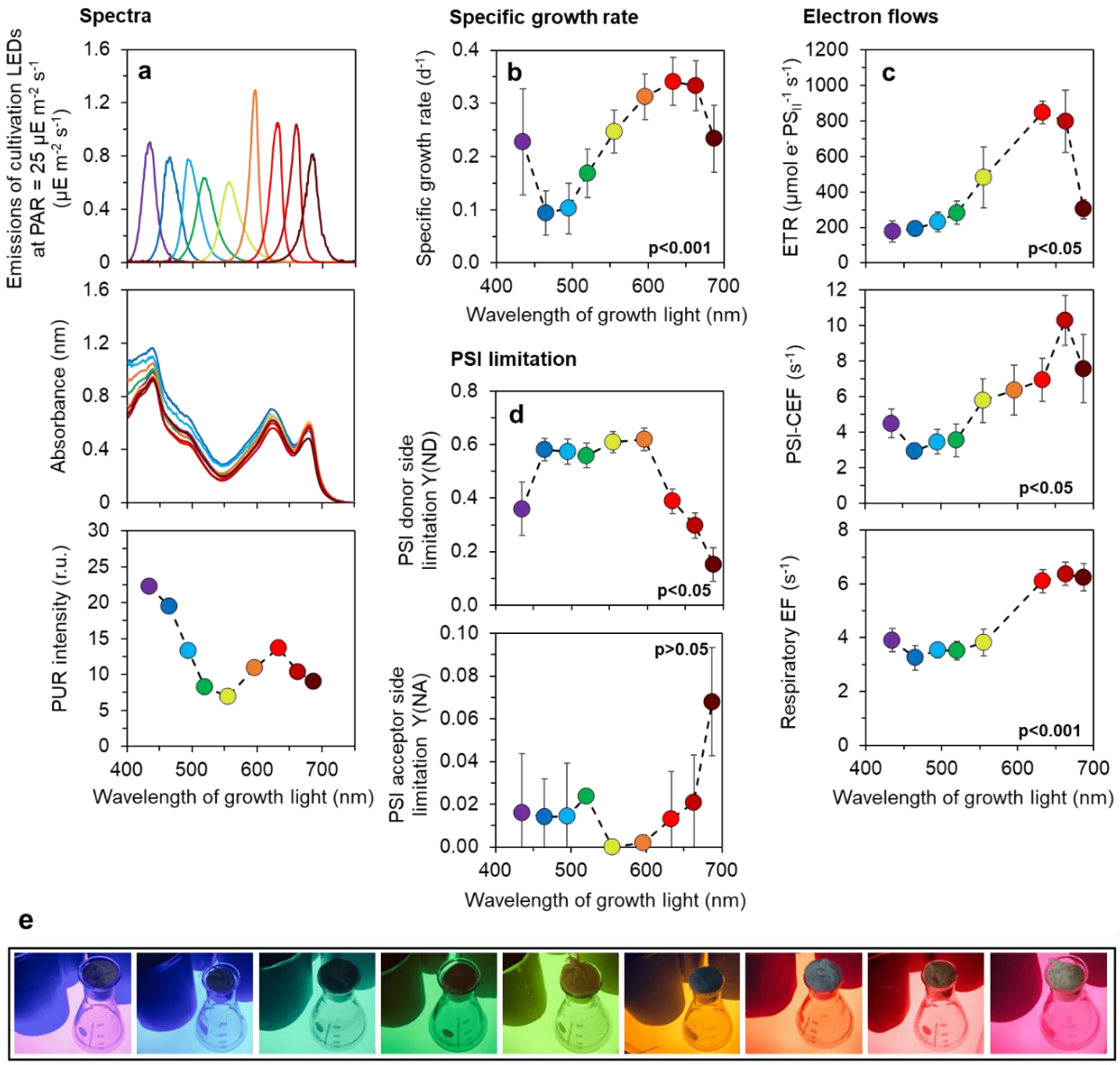

Fig. 1 **Growth rate and electron flows in *Synechocystis* cells during cultivation under monochromatic lights. a** Emission spectra of monochromatic cultivation LEDs at photosynthetically available irradiance (PAR) of 25 µmol photons m^{-2} s^{-1}, absorption spectra of *Synechocystis* cultures cultivated under individual LEDs and resulting photosynthetically usable radiation spectra. **b** Specific growth rates of *Synechocystis* cells under the monochromatic lights. **c** Electron transport rates (ETR) through PSII), cyclic electron flow around PSI (PSI-CEF), and respiratory electron flow. **d** Donor side (Y(ND) and acceptor side (Y(NA) limitation of PSI. The values in panels *a-d* represent mean±SD (n = 3-6). Values in panel *a* are shown without error bars for clarity. The p-values indicate result of Kruskal-Wallis test. **e** *Synechocystis* cultures sitting at the cultivation bench. Monochromatic light conditions were secured by covering the all Erlenmeyer flasks by black caps (also captured in the photos).

Increased electron flow under red light allows to accumulate more cellular reserves

All pigments, including PBS, Chl *a* and carotenoids were downregulated under blue light. In contrast, Chl *a* and carotenoids were upregulated under green light, and carotenoids were further upregulated under violet and near far-red light (*Fig. 2a*). The most upregulated carotenoids included echinenone, myxoxanthophyll and synechoxanthin (Supplementary Figure S1). The resulting carotenoids / Chl *a* ratio was slightly increased under violet and near far-red lights (Supplementary Figure S2). Interestingly, in spite of dramatic changes in the content of light harvesting pigments, the functional absorption cross-section of PSII (σ_{II}) was independent of cultivation wavelength (Supplementary Figure S3).

Optimal light harvesting and, in turn, efficient electron flow allowed *Synechocystis* to accumulate cellular reserves. The cellular pools of proteins, carbohydrates (but not glycogen) and lipids were upregulated under orange to red light (*Fig. 2c*; Supplementary Figure S4). As a result of these shifts, *Synechocystis* cells were larger in volume under red light (*Fig. 2b*).

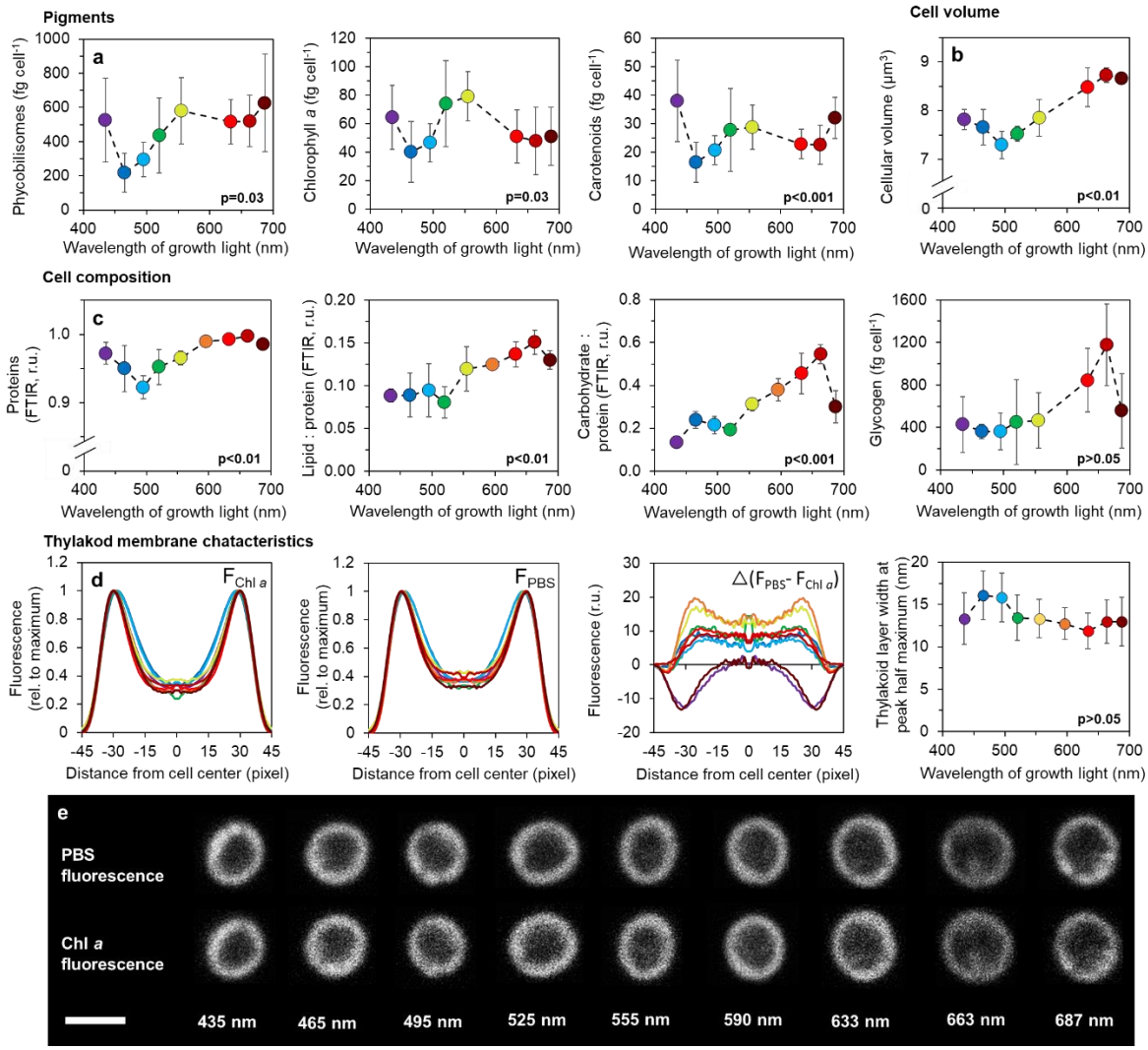

Fig. 2 **Composition and morphology of *Synechocystis* cells during cultivation under monochromatic lights. a** Content of phycobilisomes (PBS), chlorophyll *a* (Chl *a*) and carotenoids. **b** Cellular volume. **c** Content of protein, carbohydrate, lipid and glycogen in *Synechocystis* cells. **d** Parameters derived from confocal microscopy imaging: autofluorescence profiles of Chl *a* ($F_{Chl\,a}$) and PBS (F_{PBS}) across *Synechocystis* cells, difference between F_{PBS} and $F_{Chl\,a}$, and thickness of the thylakoid membrane as determined from $F_{Chl\,a}$ at half maximum of fluorescence peaks. All values represent mean±SD (n = 3–5 (a-c) / 58-113 (d-e)). Error bars in fluorescence profiles are omitted for clarity. The p-values indicate result of Kruskal-Wallis test. **e** Microscopy images of representative *Synechocystis* cells as cultivated under monochromatic lights. Scale bar: 2 µm.

Synechocystis has limited options to fine-tune light harvesting under blue light

To further understand fine-tuning of light harvesting, 3D fluorescence excitation-emission maps at 77K were recorded. Analysis of the fluorescence spectra allowed to identify PBS bound either to PSI (PBS-PSI) to PSII (PBS-PSII), and PBS that

were functionally uncoupled from both PSI and PSII (PBS-free, for details see eq. (4-6)). PBS-PSII were downregulated under blue, green and orange light (*Fig. 3a*), consistently with limitation of PSI at donor side under the same conditions (*Fig. 1c*). PBS-PSI were independent of the cultivation wavelength and PBS-free were downregulated under blue light and increased under violet light (*Fig. 3a*). Chl *a* fluorescence originating in PSII (PSII-Chl) was upregulated under both violet and red / near far-red light, whereas Chl *a* fluorescence originating in PSI (PSI-Chl) was upregulated under red but downregulated under near far-red light (Supplementary Figure S5). These results suggest distinct acclimation strategies of *Synechocystis* to violet and to near-far-red lights, even though PSI / PSII ratio was remarkably low for both violet and near far-red light acclimated cultures (*Fig. 3b*).

Increased PSII abundance under violet and near far-red lights was further confirmed by the analysis of confocal micrographs that revealed higher autofluorescence of Chl *a* over PBS under these cultivation wavelengths (*Fig. 2d*). Confocal microscopy also revealed independence of thickness of the thylakoid membranes on the cultivation wavelength (*Fig. 2d*) and further confirmed PBS localization within thylakoid membranes, opposite to *Cyanobium gracile* that was previously shown to detach PBS from the thylakoid membranes area under near far-red light (Bernát et al., 2021).

Detailed analysis of the excitation and emission spectra (as summarized in Supplementary Figure S6-S7) can reveal additional features, such as fluorescence emission originating in CP43 and CP47 proteins of PSII upon 440 nm excitation (Remelli and Santabarbara, 2018), whose ratio can provide insight into PSII lifecycle and assembly state. Even though under blue and near-far-red cultivation lights slightly increased amount of fully assembled PSII centers was found, the CP43/CP47 was independent of cultivation wavelength (Supplementary Figure S8), which suggests similar PSII turnover rate under all tested wavelengths.

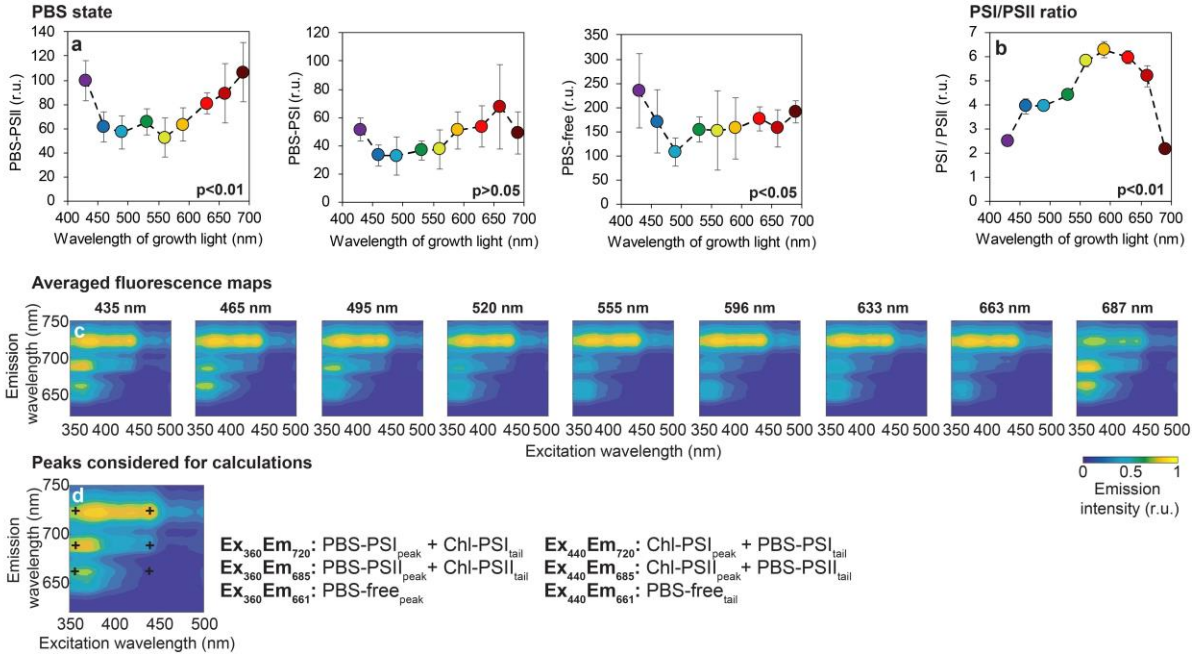

Fig. 3 **Fluorescence excitation-emission maps measured at 77K and derived parameters. a** Fluorescence of phycobilisomes (PBS) attached to PSII (PBS-PSII), to PSI (PBS-PSI), and of phycobilisomes uncoupled from both photosystems (PBS-free). **b** PSI/PSII ratio **c** Excitation-emission maps of *Synechocystis* cultures cultivated under monochromatic lights. The maps represent standardized averages (n = 3); error intervals are not shown. **d** Representative excitation-emission map with particular wavelengths considered for calculation of parameters as show in panels *a-b*. For further details on the 77K spectra processing see Methods and Supplementary methods. The values in panels *a-b* represent mean±SD (n = 5-6). The p-values indicate result of Kruskal-Wallis test.

Besides studying the functional attachment of PBS to photosystems, also the rates of state transitions were investigated by the measurement of pigment fluorescence kinetic. To induce *State 1* and *State 2*, *Synechocystis* cultures were illuminated by weak blue and red light was used respectively (*Fig. 4c*). In general, *State 2* → *State 1* transition was faster compared to *State 1* → *State 2* transition (*Fig. 4a*) at all growth wavelengths. Considering the effect of cultivation wavelength, the slowest ST rates and, hence, the less efficient capability to fine-tune the light harvesting were found under blue-green cultivation lights (*Fig. 4a*). In line with these results, NPQ (as induced by strong blue actinic light (AL), *Fig. 4a*) was also the weakest under blue cultivation light. However, the dependency of NPQ on the cultivation wavelength was slightly shifted for cultures acclimated to *State 1* and *State 2* prior to the NPQ measurement (*Fig. 4b*). Recordings of pigment fluorescence kinetic under all cultivation lights are provided in Supplementary Figure S9-S10.

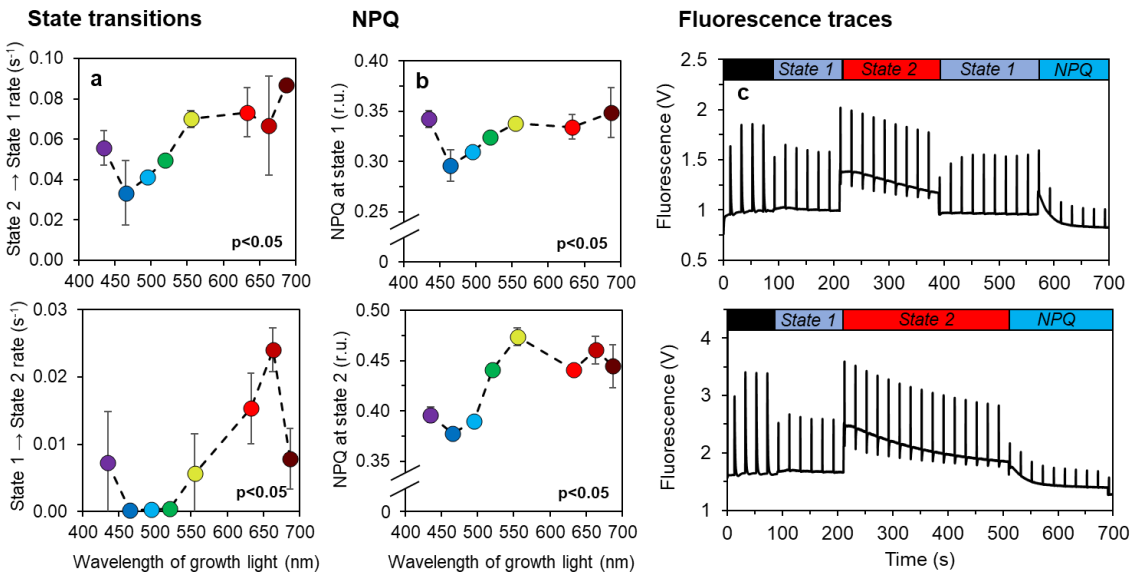

Fig. 4 **Rates of state transition and NPQ. a** Rates of transition from *State 2* to *State 1* and *State 1* to *State 2*. *State 1* and *State 2* were induced by applying weak blue and red actinic light (AL), respectively (see below). **b** Non-photochemical quenching (NPQ), induced by strong blue AL, as measured in *Synechocystis* cells in *State 1* and *State 2*. The values represent mean±SD (n = 3). The p-values indicate result of Kruskal-Wallis test. **c** Examples of fluorescence kinetics measurement protocols used for determination of *State 2* → *State 1* rate and NPQ in *State 1* (upper panel) and *State 1* → *State 2* rate and NPQ in *State 2* (lower panel). Prior to the protocol, cells were dark-acclimated for 15 min. *State 1* was induced by 80 µmol photons m^{-2} s^{-1} of 480 nm AL, while *State 2* was induced by 50 µmol photons m^{-2} s^{-1} of 625 nm AL. NPQ was triggered by 480 nm light of 1 800 µmol photons m^{-2} s^{-1}. Fluorescence traces under all cultivation wavelengths are provided in Supplementary Figure S9-S10.

Blue light leads to reduction of PQ pool and formation of ROS

Both slow and fast pigment kinetics can provide semi-quantitative information about the status of reduction state of the plastoquinone (PQ) pool. All followed parameters suggest that the PQ pool was the most reduced under blue cultivation light, and the most oxidized under red cultivation light. These include V_J-V_I slope of OJIP curves and $\triangle F(F_t\text{-}F_0)$ as well as F_0 as derived from the slow pigment fluorescence kinetics (*Fig. 5a*, Supplementary Figure S11). The redox level of the PQ pool was irrespective of whether *Synechocystis* was dark, red, or blue light. The PQ pool reduction under blue light was accompanied by high level of reactive oxygen species (ROS; *Fig. 5b*). We note, however, that the used ROS estimation method only allowed for semi-quantitative general ROS estimation (Murphy et al., 2022).

Closer analysis of the efficiency of linear electron transport rate revealed a temporal pattern in PQ pool oxidation. In cells cultivated under violet and near-far-red light, the level of pigment fluorescence right after a saturation pulse dropped transiently below the steady-state level at the onset of red AL. This drop was gradually moderated, and after 5 min of AL illumination it was negligible in all cultures (*Fig. 5c-d*). This suggests temporally limited ability of PSI to oxidize the PQ pool under violet and near-far-red light, which is likely related to increased PSII content under both abovementioned lights as well as with reduced PSI content under violet light (Supplementary Figure S5).

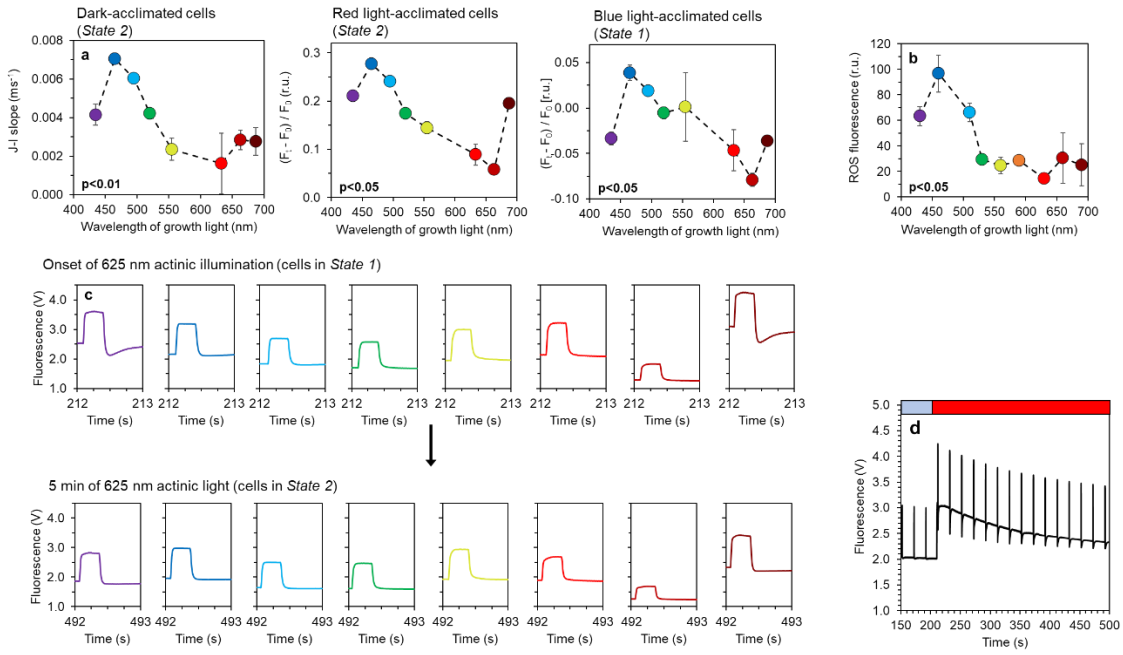

***Fig. 5* Redox state of PQ pool, formation of ROS and transient fluorescence drops after saturation pulses. a**: Redox state of PQ-pool as determined from (OJIP) and slow pigment fluorescence kinetics (Bernát et al., 2021). **b** Semi-quantitative estimation of general ROS concentration in *Synechocystis* cells cultivated under monochromatic lights. **c** Fluorescence traces during saturation pulses at the onset of 625 nm AL and after 5 min of 625 nm AL. **d** Example measurement of slow fluorescence kinetic. All values represent means (n = 3). Error bars in *a-b* represent SD, error bars in *c* are not shown for clarity. The p-values indicate result of Kruskal-Wallis test. Full traces of OJIP curves, together with F_0 and F_t values are detailed in Supplementary Figure S11. Full slow fluorescence induction curves are shown in Supplementary Figures S9-S10.

Photoacclimation patterns allow to predict spectral limitation in natural waters

A summary of all changes in *Synechocystis*, as a response to individual monochromatic cultivation lights, is provided in *Fig. 6*. In addition to understanding the complexity of light quality response in this model cyanobacterium, our results

also allow to predict spectral limitation of *Synechocystis* in natural waters. To this end, we simulated growth in seven underwater spectra as identified previously, covering (hyper)oligotrophic, mesotrophic and (hyper)eutrophic waters (Holtrop et al., 2021). The simulation was based on the results of *Synechocystis* growth under monochromatic LEDs as used in this study. The simulation predicts minimal *Synechocystis* growth limitation in eutrophic waters dominated by red light, and maximal growth limitation in oligotrophic waters dominated by blue light (*Fig. 7*).

Indeed, spectral composition might be not the primary factor driving fitness in natural waters. All experiments in this study were performed in full medium, at pH ≈ 8, at moderate temperature and without the presence of grazers; i.e. with optimized factors that often limit presence of phytoplankton in natural waters. For instance, proliferation of phytoplankton in oligotrophic waters is already limited by low concentration of nutrients, in contrast to eutrophic waters. However, the comparative setup addressing acclimation to individual wavelengths allows to understand and partially to quantify spectral limitation in the environment: the blue and green light-dominated underwater spectrum itself has a potential to reduce growth of *Synechocystis* by 50% (*Fig. 7s*).

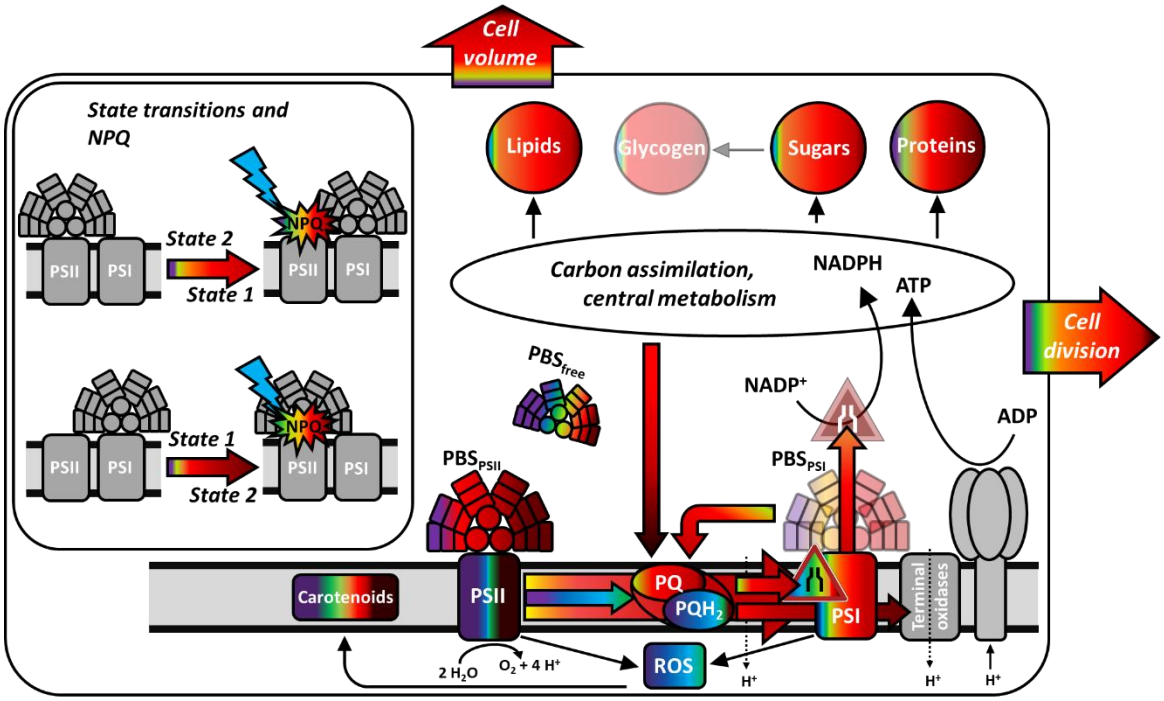

***Fig. 6* Summary of wavelength-dependent shifts in *Synechocystis* as determined in this study.** Individual processes are color-coded according to the monochromatic lights under which the particular processes were the most upregulated. Grey regions represent cellular components that were not determined (terminal oxidases, ATPase) or are depicted

only for illustrative purpose (insert showing state transition). Components / processes dependent of cultivation wavelength (based on Kruskal-Wallis test) are marked without transparency, components / processes independent of cultivation wavelengths are marked partially transparent. Colored arrows represent measured electron flows, black arrows represent pathways of which only the final sinks were determined.

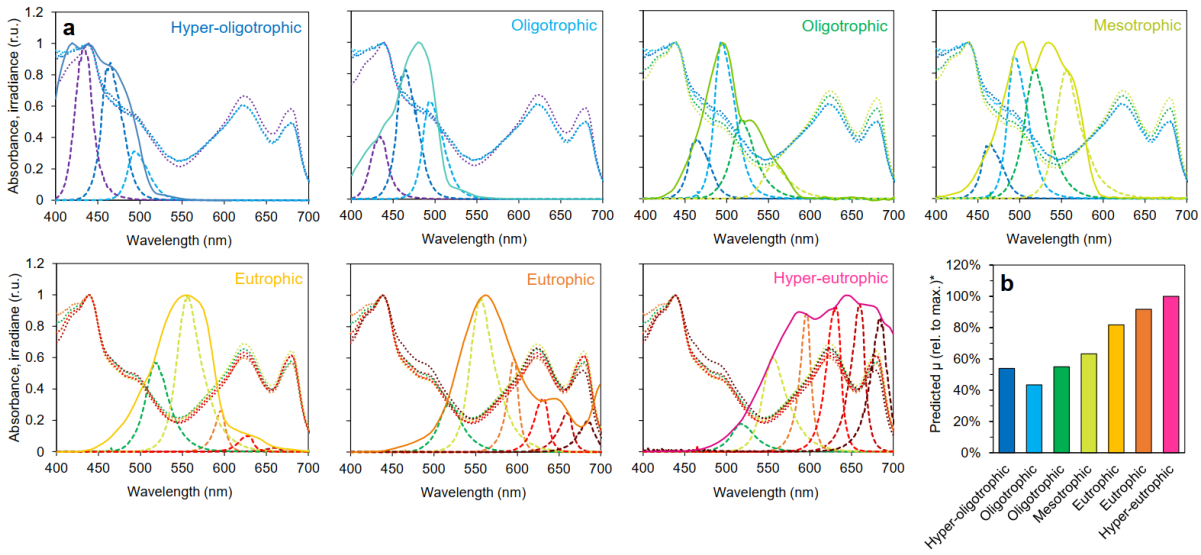

***Fig. 7* Prediction of *Synechocystis* growth in seven distinct underwater spectra.** **a** Underwater spectra in seven geographical regions as measured previously (Holtrop et al., 2021) (solid lines), emission spectra of LEDs used in this study scaled to represent particular underwater spectra (dashed lines), and absorption spectra of *Synechocystis* cells cultivated under particular monochromatic LEDs as relevant for each underwater spectrum (dotted lines). LEDs and absorption spectra are color-coded same as in Fig. 1-6. **b** Predicted growth rates of *Synechocystis* in underwater spectra, based on spectra reconstruction as shown in panel *a* and measured specific growth rates (Fig. *1*a). *The prediction is based on the conditions used in this study and assumes full medium, pH ≈ 8, moderate temperature and absence of grazers.

Discussion

In this work, light quality acclimation in the model cyanobacterium *Synechocystis* was studied. The experimental setup covering the whole spectrum of visible light (*Fig. 1*) represents a significant improvement over many previous studies, where typically only two or three wavelengths were compared. Indeed, in case of PC-containing cyanobacteria such as *Synechocystis*, cultivation under blue and red light induces two fundamentally different photoacclimation states (Luimstra et al., 2020, 2019, 2018; Singh et al., 2009), which was also confirmed here. However, this study shows that although some parameters shifted between red and blue cultivation lights

almost linearly (including growth rate, LEF, cell size, or reduction state of PQ pool), wavelength dependency of many other parameters was highly non-linear.

In addition, the range of previously studied wavelengths was extended by addressing acclimations to violet and near far-red lights. Both these lights were utilized well by *Synechocystis* (although less efficiently compared to red light), and both lead to specific responses compared to other wavelengths (such as PSI/PSII ratio). The relatively fast growth and metabolic rates of the cells under near-far-red light are likely a result of overlapping emissions of “687 nm” and “663 nm” LEDs (*Fig. 1*). Absorption of true far-red light (> 700 nm) is quite inefficient in *Synechocystis*, and growth rate under far-red light is similar as under blue light (Wilde et al., 1997). Moreover, far-red light induces complex transcription shift that generally resembles stress response (Hübschmann et al., 2005) – which is also common for blue light acclimation (Luimstra et al., 2020; Singh et al., 2009).

On the other hand, increased growth rate under violet (435 nm) LED compared to blue (465 nm) LED was likely a result of higher PUR (*Fig. 1*). Interestingly, the higher growth rate was accompanied by slightly increased PSI-CEF and REF, but not LEF under violet light (compared to blue light), showing potential of these processes for growth optimization. Both violet and near far-red light resulted in increased abundance of PSII and PBS-PSII (*Fig. 3*, Supplementary Figure S5) that helped to overcome the donor-side limitation of PSI (Y(ND); *Fig. 1*). In addition, synthesis of xanthophylls but not β–carotene was upregulated under both these lights (Supplementary Figure S1) which suggests alterations in thylakoid membrane structure under violet and near far-red lights (Rodrigues et al., 2023; Zakar et al., 2017).

Blue light is known to induce a wide range of acclimation responses in *Synechocystis* (Luimstra et al., 2020, 2019, 2018; Singh et al., 2009), mainly as a result of the inability to provide enough reducing equivalents such as NADPH and/or Fd_{red} *via* LEF (Singh et al., 2009), together with the inability to generate enough ATP (Luimstra et al., 2020). The low LEF under blue photons was also measured here (*Fig. 1*), together with high PQ pool reduction (*Fig. 5*; Supplementary Figure S11). Closer look on the efficiency of electrons transfer from PSII to PSI acceptors revealed that under blue light PSII-trapped electrons were transferred efficiently from

Q_A^- to PQ (ψE_0) but inefficiently from PQH_2 to final acceptors (δR_0; Supplementary Figure S12), similarly as in *Cyanobium gracile*, a close relative of *Synechocystis* (Bernát et al., 2021).

The PQ pool reduction under blue light (as confirmed by increased F_0, $\Delta(F_t\text{-}F_0)$ and V_J; *Fig. 5*, Supplementary Figure S11) and, in turn, ROS formation, could potentially be related to the saturation of sink capacity of the Calvin–Benson–Bassham (CBB) cycle. However, carbon-concentrating mechanism (CCM) was found to be upregulated under blue light previously (Singh et al., 2009). In line with that, and consistently with previous works (Allahverdiyeva et al., 2011), we found only negligible limitation of PSI on the acceptor side (*Fig. 1*). Another possible cause for inefficient electron transfer from PQH_2 to terminal acceptors is downregulation of the cytochrome b_6f complex. However, this (central) component of the photosynthetic electron transport chain (PSET) was found upregulated under blue light previously (Singh et al., 2009). Alternative hypotheses include reduced level of PSI and/or terminal respiratory oxidases, as well as additional electron fluxes from Fd_{red}, succinate, plastocyanin, ferredoxin-$NADP^+$ reductase, or NAD(P)H dehydrogenase NDH-1 (Deák et al., 2014). Since these fluxes were not addressed in this study (with the exception of respiratory electron flow, *Fig. 1*), the origin of the reduced PQ pool under blue light, even with low activity of PSII, PSI and respiration, remains an open question. However, this phenomenon has been described also for another cyanobacterium recently (Bernát et al., 2021).

Furthermore, under blue light we found strongly downregulated APC levels (Supplementary Figure S13), suggesting inefficient PBS binding to both PSII and PSI (as confirmed in *Fig. 3)*. Transcript levels of APC genes were found to be upregulated under blue light in previous works, together with transcription of PBS degradation genes (Luimstra et al., 2020; Singh et al., 2009). It is therefore likely that the APC downregulation under blue light as measured here was related to post-transcriptional or (post-)translational regulation. The APC shortage can also explain low kinetic rates of ST under blue and green light (*Fig. 4*). ST become relevant for light energy distribution only when PBS are in the canonical form (i.e. CpcG1 form, (Kondo et al., 2009)) which was feasible here only under when APC was not limited (Supplementary Figure S15). Analogously, the APC shortage can also explain reduced NPQ under blue light (*Fig. 4*).

Many measured trends were different between blue and green cultivation lights, despite the fact that there was an overlap in the emission spectrum of “495 nm” and “520 nm” LEDs (*Fig. 1*). Under green light, a specific PBS form called CpcL-PBS is able to bind to PSI through CpcL linker (Kondo et al., 2009). Such CpcL-PBS-PSI binding is not known to exist under blue light. With shift from blue to green wavelength, PBS can thus absorb more light through APC and the absorbed energy can be then transferred to PSI *via* CpcL-PBS.

In contrast to blue light, the fastest growth was found under orange/red light. These wavelengths were optimal for generating both energy and reducing equivalents through LEF, PSI-CEF and REF (*Fig. 1*). The results of this study show that it is not only the absolute number of photosystems or light-harvesting antenna, or PBS attachment to PSII or PSI, but rather a balance of many individual parameters that allows to optimize production and ratio of ATP and NADPH and cellular growth. A wide range of processes is optimized under red light, as summarized in the previous works (Luimstra et al., 2020; Singh et al., 2009; Wiltbank and Kehoe, 2019). Efficient red light capture by PBS allows to further optimize light harvesting through state transitions (*Fig. 4*) as well as through carbohydrates or lipid synthesis (*Fig. 2*).

Results of this study also allowed to predict growth limitation of PC but not phycoerythrin (PE)-containing CA1-type cyanobacteria in environments with shifted underwater spectra (*Fig. 7*). Indeed, these predictions are partly reliant on growth conditions, and the wavelength dependency of growth could possibly change with the increase in temperature, salinity or irradiance (Zavřel et al., 2017). In addition, it has been shown that using ammonia instead of nitrate can result in a significant increase in growth rate of *Synechocystis* under blue light (Singh et al., 2009).

By addressing spectral dependency of light harvesting, electron transport and energy storage within cells, this work provides insight into spectral limitations of CA1-type, PC-rich cyanobacteria in natural environments. The results can straighten design of new strains towards improved light utilization for the synthesis of targeted products. A call for such optimization has been announced (Klaus et al., 2022), and a proof-of-concept study addressing the effect of light quality on the synthesis of bulk chemicals has been provided recently (Rodrigues et al., 2023).

Materials and Methods

Inoculum cultures and experimental setup

All cultivations of *Synechocystis* sp. PCC 6803 GT-L (Zavřel et al., 2015a) were performed in batch regime in conical flasks on air at 24 °C in BG-11 medium (van Alphen et al., 2018) under light-dark regime set to 14:10 h. All cultures were sitting on a cultivation bench and were shaken daily to prevent excessive sedimentation of the cells. The inoculum cultures were cultivated under cool-white fluorescent lamps (25 µmol photons m^{-2} s^{-1}). Prior to the cultivations under monochromatic LEDs, cultures were diluted with fresh BG-11 such that the optical density at 750 nm (Specord 210 plus, Analytik Jena, Germany) at the day of sampling was OD_{750} = 0.2 for all cultures.

During the experiments under monochromatic LEDs, illumination was secured by a home-built cultivation bench apparatus with 9 monochromatic LEDs (for spectra, see *Fig. 1a*): FD-34UV-Y1 (peak wavelength: 435 nm), FD-3B-Y1 (465 nm), FD-32G-Y1 (495 nm), FD-3GY1 (520 nm), B08QCMC3K1 (555 nm), FD-3Y-Y1 (596 nm), FD-3R-Y1 (633 nm), FD-333R-Y1 (663 nm) and FD-34R-Y1 (687 nm). All LEDs but 555 nm LEDs were manufactured by Shenzhen Fedy Technology Co. (Shenzhen, China). The 555 nm LED was manufactured by Nagulagu Co., Ltd. (Shenzhen, China). The PAR intensity of each diffused LED light was set to 25 µmol photons m^{-2} s^{-1}.

Growth rates, cell size and cell composition

Specific growth rates were calculated from OD_{750} (Specord 210 plus) using exponential regression model. Cell size was determined by ImageStream MkII imaging flow cytometer (Amnis Corp., Seattle, WA, United States) using a previously described method (Zavřel et al., 2019). Briefly, samples were treated with 2% formaldehyde, incubated for 10 min at room temperature and stored at –80°C. Prior to the analysis, samples were thawed at room temperature (~ 30 min) and processed by flow cytometry to discriminate (i) focused objects and (ii) round objects (width/length ratio 0.9-1.0). During cytometric analysis, pigment autofluorescence (excitation: 642 nm, detection: 642–745 nm) was also recorded to validate selection of cells within all measured objects. Bright field images were used for cell size analysis, cellular shape was assumed spherical.

The relative abundance of proteins, lipids and carbohydrates was estimated by Fourier Transformed Infrared Spectroscopy (FTIR), following the previously described protocol (Felcmanová et al., 2017). Briefly, 5 mL of the culture suspension was centrifuged (4 000 x *g*, 5 min), supernatant was discarded, pellet was freeze-dried, and dry pellet was analyzed by a Nicolet IS10 spectrometer (Thermo Fisher Scientific, Waltham, MA, USA).

Content of glycogen, Chl *a*, total carotenoids and PBS was measured by previously described protocols (Zavřel et al., 2018b, 2018a, 2015b). To distinguish the contribution of individual carotenoids to the total carotenoid pool, additional analysis was performed using high-performance liquid chromatography (HPLC) and previously developed method (Bernát et al., 2021). Briefly, 10 mL cultures aliquots were harvested (Whatman glass microfiber filters GF/B; ⌀ 25 mm) and stored at –80°C. Soluble pigments were extracted in 500 µL of acetone and analyzed by a Shimadzu Prominence HPLC system (Shimadzu, Kyoto, Japan). Pigments separation was carried out on a Phenomenex Synergi 4 µm Hydro-RP 80 Å, LC Column 150 x 4.6 mm at 25°C. 20 µL aliquots were injected and the pigments were eluted by a linear gradient from solvent A (acetonitrile, water, trimethylamine; in a ratio of 9:1:0.01) to solvent B (ethyl acetate) at a flow rate of 1 mL min^{-1} (total time: 25 min). Pigments were identified according to the respective retention times and absorption spectra, and quantified by integrated chromatographic peak areas.

Photosynthetic Activity Measurements

PSII activity was probed by Multi-Color-PAM (MC-PAM; Walz, Effeltrich, Germany) using both slow (*SP-Analysis*) and fast fluorescence induction kinetics (*Fast Acquisition*), 625 nm measuring light (ML) and 15 min of dark acclimation.

During slow kinetics, actinic light (AL) of 480 nm (inducing *State 1*) or 625 nm (inducing *State 2* (Calzadilla and Kirilovsky, 2020)) was used, with intensities of 80 µmol photons m^{-2} s^{-1} and 50 µmol photons m^{-2} s^{-1}, respectively (both sufficiently high to induce fluorescence transients). To induce NPQ, 480 nm light of intensity 1 800 µmol photons m^{-2} s^{-1} was additionally used. To calculate ETR, functional absorption cross-section of PSII (σ_{II}) was determined, using the default MC-PAM script *Sigma1000cyano*. In MC-PAM, the wavelength of AL defines also wavelength of saturation pulses (SP). It has to be noted that even the highest SP intensity (SP-

int=20) at 480 nm was not strong enough to provide full PSII saturation, in contrast to SP of 625 nm (Supplementary Figure S14).

OJIP curves were recorded using *FastKin_Def* trigger settings and 625 nm saturation pulses. The efficiency of e^- transport from Q_A^- to PQ (ψE_0) and from PQH_2 to final acceptors (δR_0) was calculated from V_J (2 ms) and V_I (30 ms) points of the OJIP curves (Supplementary Figure S11) according to (Stirbet et al., 2018):

$$\psi E_0 = 1 - V_J \quad (1)$$

$$\delta R_0 = (1 - V_I) / \psi E_0 \quad (2)$$

Redox state of PQ pool was estimated semi-quantitatively 1) from OJIP curves as a rate of fluorescence rise between V_J and V_I, 2) from slow kinetic measurements from F_0 values (steady-state fluorescence after 15 min of dark acclimation), and 3) from slow kinetics measurements as a difference between F_0 and Ft (fluorescence level at the end of *State 2* or *State 1* AL periods at 500 s and 570 s of the slow kinetic recordings (Supplementary Figure S9 and 10, respectively).

PSI kinetics was probed by a Dual-PAM-100 fluorometer (Walz, Effeltrich, Germany). Culture aliquots were filtered through glass fiber filters (GF/B, Whatham). Wet filters were placed between two microscope glass slides within the leaf holder DUAL-B (Supplementary Figure S15) and dark-acclimated for 10 min. PSI limitation on both donor and acceptor sites was probed by *SP-analysis* mode (using *Fluo+P700 Measuring mode*). Rate of electrons transport through PSI was measured by *FastAcquisition* mode in the absence of inhibitors (total electron flow through PSI), in the presence of 10 µM DCMU (inhibiting electron flow through PSII and thus estimating cyclic electron flow around PSI, PSI-CEF) and in the presence of 10 µM DCMU + 100 µM methyl-viologen (MV, a high affinity acceptor of PSI electrons) to quantify respiratory electron flow, by inhibiting PSII by DCMU and effectively preventing PSI-CEF by MV.

Absorption and excitation-emission spectroscopy

Whole cell absorption spectra were recorded by Specord 210 plus spectrophotometer (Analytik Jena). To correct for light scattering by the cellular matter, four slices of tracing paper were placed in front of both sample and reference

cuvettes. The measured spectra (offset-corrected) were used to calculate PUR (Photosynthetically Usable Radiation) of each monochromatic LED as:

$$PUR_{400}^{750} = PAR_{400}^{750} * abs_{400}^{750}, \quad (3)$$

where PAR_{400}^{750} and abs_{400}^{750} represent photosynthetically active radiation spectra of cultivation LEDs and absorbance spectra of *Synechocystis* cultures under the particular LED, respectively, in range 400-750 nm.

Fluorescence excitation-emission maps were recorded by Jasco FP-8550 spectrofluorometer (Jasco, Tokyo, Japan) at 77K. 10 mL culture aliquots were filtered (GF/B filters, Whatman, Maidstone, UK), flash-frozen in liquid nitrogen and stored at -80 °C. Before spectra recording, a slice from each filter (~1 cm × 0.3 cm) was cut to fit the metal holder of the transparent Dewar flask. 77K (3D) spectra were recorded in excitation range 350 nm - 650 nm (step: 5 nm) and emission range 620 nm - 800 nm (step: 0.5 nm, bandwidth 5 nm, scan speed 1 000 nm min^{-1}, sensitivity low). To distinguish fluorescence originating in phycobilisomes attached to PSII (PBS-PSI), to PSI (PBS-PSI), phycobilisomes functionally uncoupled from both photosystems (PBS-free) as well as chlorophyll *a* fluorescence originating in PSII (Chl-PSII) and PSI (Chl-PSI), following equations were used (Luimstra et al., 2020; Zavřel et al., 2021):

$$PBS - free = Ex_{360}\, Em_{661} \quad (4)$$

$$PBS - PSII = 0.937 * Ex_{360}\, Em_{695} - 0.695 * Ex_{440}\, Em_{695} \quad (5)$$

$$PBS - PSI = 0.937 * Ex_{360}\, Em_{726} - 0.695 * Ex_{440}\, Em_{726} \quad (6)$$

$$Chl\ a - PSII = 1.063 * Ex_{440}\, Em_{695} - 0.0696 * Ex_{360}\, Em_{695} \quad (7)$$

$$Chl\ a - PSI = 0.937 * Ex_{440}\, Em_{726} - 0.695 * Ex_{360}\, Em_{726} \quad (8)$$

$$PSI/PSII = \frac{Chl\ a - PSI}{Chl\ a - PSII}, \quad (9)$$

where Ex_{360} and Ex_{440} represent excitation at 360 nm and 440 nm (preferentially exciting PBS and Chl *a*, respectively), and Em_{661}, Em_{695} and Em_{726} represent fluorescence emission by PBS, PSII and PSI, respectively. The coefficients of Eq. (4-8) include correction of fluorescence emission leaking between 360 and 440 nm (PBS

and Chl *a* fluorescence tails), based on the analysis of fluorescence maps of *Synechocystis* sp. PCC 6803 WT and PAL mutant lacking phycobilisomes (Ajlani and Vernotte, 1998) (Supplementary Figure S16). Further details of the selection of particular excitation-emission peaks are shown in *Fig. 3*.

Confocal microscopy

Microscopy imaging was performed using a TCS SP8 DMI confocal laser scanning microscope (Leica Microsystems Inc. Wetzlar, Germany) equipped with a HC PL APO CS2 63×/1.4 oil immersion objective and a TD 488/552/638 main beam splitter. 10 mL culture aliquots were centrifuged (2500 x *g*, 5 min, 25 °C), supernatant was partially discarded and 10 µL of the concentrated sample was immobilized on a thin (<1 mm) layer of solid BG-11 agar and placed upside down on a cover slide. Chl *a* and PBS autofluorescence were excited using 488 nm and 638 nm lasers, respectively, and detected over 690–790 nm and 650–680 nm spectral windows. The recorded images were processed by self-developed Matlab script that allowed for evaluation of both Chl *a* and PBS fluorescence profiles within each identified cell (by setting with 5° step, each cell was divided into 72 circular sectors around its geometrical center).

Measurement of reactive oxygen species (ROS)

ROS were measured non-specifically and semi-quantitatively, according to established protocols (Hakkila et al., 2014; Thiel et al., 2017). Cultures were centrifuged (3000 *x* g, 5 min) and resuspended in fresh BG-11 medium in a final volume of 1 mL. Samples were incubated with 25 µM 2′,7′-dichlorodihydrofluorescein diacetate (H_2DCFDA) for 90 min in dark and washed with fresh BG-11 same as described above. 200 µL aliquot of each sample was pipetted to black 96 well plate, together with blanks (BG-11+25 µM H_2DCFDA). Measurements were performed first on the dark-acclimated samples using a Victor 3 plate-reader (Perkin Elmer, Waltham, MA, United States), 485 nm excitation and 535 nm and 680 nm emission (H_2DCFDA and pigment fluorescence, respectively). Subsequently, samples were placed for the light treatments at the respective cultivation wavelengths for 120 min. After the light treatment, 200 µL aliquots were loaded to the well plates and fluorescence measurements were performed again as described above. H_2DCFDA fluorescence of *Synechocystis* cells was normalized to 680 nm fluorescence and corrected for blank

fluorescence in all cases. The measurement setup allowed to prevent artifacts related to shifts in dissolved O_2 or pH (Murphy et al., 2022).

Statistical analysis

To identify parameters that significantly varied between the light conditions, Kruskal-Wallis test was performed (Statistica, TIBCO, USA), by a pair-by-pair comparing of all tested monochromatic lights. Null hypothesis was that the median of all compared groups was equal. Parameters identified as significantly changing between the lights were those that had at least one pair that differed significantly with a p-value < 0.05 ($n = 3–9$ for all lights throughout all experiments).

Data Availability

The data underlying this article are available in the Figshare repository at 10.6084/m9.figshare.23330363.v1.

Funding

This work was financially supported by the Ministry of Education, Youth and Sports of CR within the CzeCOS program (grant number LM2018123) and under the OP RDE (grant number CZ.02.1.01/0.0/0.0/16_026/0008413 ‘Strategic Partnership for Environmental Technologies and Energy Production’) as well as by the National Research, Development and Innovation Office of Hungary, NKFIH (awards K 140351 and RRF-2.3.1-21-2022-00014 to G.B. and B.S.).

Acknowledgement

We thank Tímea Szabó, Balázs Németh, and Máté Burányi for their technical assistance. We are grateful to János Győri and Anna Felpéczi-Farkas from Balaton Limnological Research Institute for providing us the access to the Victor 3 fluorescence plate-reader.

Author Contributions

T.Z., and G.B. designed and performed experiments and/or generated material; T.Z., A.S., L.K., M.L., Z.N., M.S., B.S., O.P., J.Č., and G.B. designed experiments, analyzed data, and discussed results; T.Z. wrote the initial draft of the article; A.S., L.K., M.L., Z.N., M.S., B.S., O.P., J.Č., and G.B. contributed to finalizing the article.

Disclosures

Conflicts of interest: No conflicts of interest declared

References

Ajlani, G., Vernotte, C., 1998. Construction and characterization of a phycobiliprotein-less mutant of Synechocystis sp. PCC 6803. Plant Mol. Biol. 37, 577–580.

Allahverdiyeva, Y., Ermakova, M., Eisenhut, M., Zhang, P., Richaud, P., Hagemann, M., Cournac, L., Aro, E.M., 2011. Interplay between flavodiiron proteins and photorespiration in Synechocystis sp. PCC 6803. J. Biol. Chem. 286, 24007–24014.

Bernát, G., Zavřel, T., Kotabová, E., Kovács, L., Steinbach, G., Vörös, L., Prášil, O., Somogyi, B., Tóth, V.R., 2021. Photomorphogenesis in the Picocyanobacterium Cyanobium gracile Includes Increased Phycobilisome Abundance Under Blue Light, Phycobilisome Decoupling Under Near Far-Red Light, and Wavelength-Specific Photoprotective Strategies. Front. Plant Sci. 12, 1–16.

Calzadilla, P.I., Kirilovsky, D., 2020. Revisiting cyanobacterial state transitions. Photochem. Photobiol. Sci. 19, 585–603.

Cano, M., Holland, S.C., Artier, J., Burnap, R.L., Ghirardi, M., Morgan, J.A., Yu, J., 2018. Glycogen Synthesis and Metabolite Overflow Contribute to Energy Balancing in Cyanobacteria. Cell Rep. 23, 667–672.

Deák, Z., Sass, L., Kiss, É., Vass, I., 2014. Characterization of wave phenomena in the relaxation of flash-induced chlorophyll fluorescence yield in cyanobacteria.

Biochim. Biophys. Acta - Bioenerg. 1837, 1522–1532.

Demmig-Adams, B., Adams, W.W., 2006. Photoprotection in an ecological context: the remarkable complexity of thermal energy dissipation. New Phytol. 172, 11–21.

Felcmanová, K., Lukeš, M., Kotabová, E., Lawrenz, E., Halsey, K.H., Prášil, O., 2017. Carbon use efficiencies and allocation strategies in Prochlorococcus marinus strain PCC 9511 during nitrogen-limited growth. Photosynth. Res. 134, 71–82.

Grébert, T., Doré, H., Partensky, F., Farrant, G.K., Boss, E.S., Picheral, M., Guidi, L., Pesant, S., Scanlan, D.J., Wincker, P., Acinas, S.G., Kehoe, D.M., Garczarek, L., 2018. Light color acclimation is a key process in the global ocean distribution of Synechococcus cyanobacteria. Proc. Natl. Acad. Sci. U. S. A. 115, E2010–E2019.

Grébert, T., Nguyen, A.A., Pokhrel, S., Joseph, K.L., Ratin, M., Dufour, L., Chen, B., Haney, A.M., Karty, J.A., Trinidad, J.C., Garczarek, L., Schluchter, W.M., Kehoe, D.M., Partensky, F., 2021. Molecular bases of an alternative dual-enzyme system for light color acclimation of marine Synechococcus cyanobacteria. Proc. Natl. Acad. Sci. U. S. A. 118, 1–8.

Hakkila, K., Antal, T., Rehman, A.U., Kurkela, J., Wada, H., Vass, I., Tyystjärvi, E., Tyystjärvi, T., 2014. Oxidative stress and photoinhibition can be separated in the cyanobacterium Synechocystis sp. PCC 6803. Biochim. Biophys. Acta - Bioenerg. 1837, 217–225.

Hirose, Y., Chihong, S., Watanabe, M., Yonekawa, C., Murata, K., Ikeuchi, M., Eki, T., 2019. Diverse Chromatic Acclimation Processes Regulating Phycoerythrocyanin and Rod-Shaped Phycobilisome in Cyanobacteria. Mol. Plant 12, 715–725.

Holtrop, T., Huisman, J., Stomp, M., Biersteker, L., Aerts, J., Grébert, T., Partensky, F., Garczarek, L., Woerd, H.J. van der, 2021. Vibrational modes of water predict spectral niches for photosynthesis in lakes and oceans. Nat. Ecol. Evol. 5, 55–66.

Hübschmann, T., Yamamoto, H., Gieler, T., Murata, N., Börner, T., 2005. Red and far-red light alter the transcript profile in the cyanobacterium Synechocystis sp. PCC 6803: impact of cyanobacterial phytochromes. FEBS Lett. 579, 1613–8.

Kirilovsky, D., Kerfeld, C.A., 2016. Cyanobacterial photoprotection by the orange carotenoid protein. Nat. Plants 2.

Kirk, J.T.O., 2011. Light and Photosynthesis in Aquatic Ecosystems, Third edit. ed. Cambridge University Press, Cambridge (U.K.), Cambridge.

Klaus, O., Hilgers, F., Nakielski, A., Hasenklever, D., Jaeger, K.E., Axmann, I.M., Drepper, T., 2022. Engineering phototrophic bacteria for the production of terpenoids. Curr. Opin. Biotechnol. 77, 102764.

Kondo, K., Mullineaux, C.W., Ikeuchi, M., 2009. Distinct roles of CpcG1-phycobilisome and CpcG2-phycobilisome in state transitions in a cyanobacterium Synechocystis sp. PCC 6803. Photosynth. Res. 99, 217–225.

Kumar, V., Maurya, P.K., Mondal, S., Sinha, R.P., Singh, S.P., 2018. Photomorphogenesis in the Cyanobacterium Fremyella diplosiphon Improves Photosynthetic Efficiency, Cyanobacteria: From Basic Science to Applications. Elsevier Inc.

Luimstra, V.M., Schuurmans, J.M., de Carvalho, C.F.M., Matthijs, H.C.P., Hellingwerf, K.J., Huisman, J., 2019. Exploring the low photosynthetic efficiency of cyanobacteria in blue light using a mutant lacking phycobilisomes. Photosynth. Res. 141, 291–301.

Luimstra, V.M., Schuurmans, J.M., Hellingwerf, K.J., Matthijs, H.C.P., Huisman, J., 2020. Blue light induces major changes in the gene expression profile of the cyanobacterium Synechocystis sp. PCC 6803. Physiol. Plant. 170, 10–26.

Luimstra, V.M., Schuurmans, J.M., Verschoor, A.M., Hellingwerf, K.J., Huisman, J., Matthijs, H.C.P., 2018. Blue light reduces photosynthetic efficiency of cyanobacteria through an imbalance between photosystems I and II. Photosynth. Res. 138, 177–189.

Montgomery, B.L., 2016. Mechanisms and fitness implications of photomorphogenesis during chromatic acclimation in cyanobacteria. J. Exp. Bot.

67, 4079–4090.

Müller, S., Zavřel, T., Červený, J., 2019. Towards a quantitative assessment of inorganic carbon cycling in photosynthetic microorganisms. Eng. Life Sci. 19, 955–967.

Murphy, M.P., Bayir, H., Belousov, V., Chang, C.J., Davies, K.J.A., Davies, M.J., Dick, T.P., Finkel, T., Forman, H.J., Janssen-Heininger, Y., Gems, D., Kagan, V.E., Kalyanaraman, B., Larsson, N.G., Milne, G.L., Nyström, T., Poulsen, H.E., Radi, R., Van Remmen, H., Schumacker, P.T., Thornalley, P.J., Toyokuni, S., Winterbourn, C.C., Yin, H., Halliwell, B., 2022. Guidelines for measuring reactive oxygen species and oxidative damage in cells and in vivo. Nat. Metab. 4, 651–662.

Pospíšil, P., 2012. Molecular mechanisms of production and scavenging of reactive oxygen species by photosystem II. Biochim. Biophys. Acta - Bioenerg. 1817, 218–231.

Remelli, W., Santabarbara, S., 2018. Excitation and emission wavelength dependence of fluorescence spectra in whole cells of the cyanobacterium Synechocystis sp . PPC6803 : Influence on the estimation of Photosystem II maximal quantum efficiency. BBA - Bioenerg. 1859, 1207–1222.

Rodrigues, J.S., Kovács, L., Lukeš, M., Höper, R., Steuer, R., Červený, J., Lindberg, P., Zavřel, T., 2023. Characterizing isoprene production in cyanobacteria – Insights into the effects of light, temperature, and isoprene on Synechocystis sp. PCC 6803. Bioresour. Technol. 380, 129068.

Sanfilippo, J.E., Garczarek, L., Partensky, F., Kehoe, D.M., 2019. Chromatic acclimation in cyanobacteria: A diverse and widespread process for optimizing photosynthesis. Annu. Rev. Microbiol. 73, 407–433.

Singh, A.K., Bhattacharyya-Pakrasi, M., Elvitigala, T., Ghosh, B., Aurora, R., Pakrasi, H.B., 2009. A systems-level analysis of the effects of light quality on the metabolism of a cyanobacterium. Plant Physiol. 151, 1596–608.

Stirbet, A., Lazár, D., Kromdijk, J., Govindjee, 2018. Chlorophyll a fluorescence induction: Can just a one-second measurement be used to quantify abiotic

stress responses? Photosynthetica 56, 86–104.

Tamary, E., Kiss, V., Nevo, R., Adam, Z., Bernát, G., Rexroth, S., Rögner, M., Reich, Z., 2012. Structural and functional alterations of cyanobacterial phycobilisomes induced by high-light stress. Biochim. Biophys. Acta - Bioenerg. 1817, 319–327.

Tchernov, D., Silverman, J., Luz, B., Reinhold, L., Kaplan, A., 2003. Massive light-dependent cycling of inorganic carbon between oxygenic photosynthetic microorganisms and their surroundings. Photosynth. Res. 77, 95–103.

Thiel, K., Vuorio, E., Aro, E.M., Kallio, P.T., 2017. The effect of enhanced acetate influx on Synechocystis sp. PCC 6803 metabolism. Microb. Cell Fact. 16, 1–12.

van Alphen, P., Abedini Najafabadi, H., Branco dos Santos, F., Hellingwerf, K.J., 2018. Increasing the Photoautotrophic Growth Rate of Synechocystis sp. PCC 6803 by Identifying the Limitations of Its Cultivation. Biotechnol. J. 13, 1–8.

Wang, F., Chen, M., 2022. Chromatic Acclimation Processes and Their Relationships with Phycobiliprotein Complexes. Microorganisms 10, 1562.

Wilde, A., Churin, Y., Schubert, H., Börner, T., 1997. Disruption of a Synechocystis sp. PCC 6803 gene with partial similarity to phytochrome genes alters growth under changing light qualities. FEBS Lett. 406, 89–92.

Wiltbank, L.B., Kehoe, D.M., 2019. Diverse light responses of cyanobacteria mediated by phytochrome superfamily photoreceptors. Nat. Rev. Microbiol. 17, 37–50.

Zakar, T., Herman, E., Vajravel, S., Kovacs, L., Knoppová, J., Komenda, J., Domonkos, I., Kis, M., Gombos, Z., Laczko-Dobos, H., 2017. Lipid and carotenoid cooperation-driven adaptation to light and temperature stress in Synechocystis sp. PCC6803. Biochim. Biophys. Acta - Bioenerg. 1858, 337–350.

Zavřel, T., Chmelík, D., Sinetova, M.A., Červený, J., 2018a. Spectrophotometric Determination of Phycobiliprotein Content in Cyanobacterium Synechocystis. J. Vis. Exp. 1–9.

Zavřel, T., Faizi, M., Loureiro, C., Sinetova, M., Zorina, A., Poschmann, G., Stühler, K., Steuer, R., Červený, J., 2019. Quantitative insights into the cyanobacterial

cell economy. Elife 8, 1–29.

Zavřel, T., Očenášová, P., Červený, J., 2017. Phenotypic characterization of Synechocystis sp. PCC 6803 substrains reveals differences in sensitivity to abiotic stress. PLoS One 12, e0189130.

Zavřel, T., Očenášová, P., Sinetova, M., Červený, J., 2018b. Determination of Storage (Starch/Glycogen) and Total Saccharides Content in Algae and Cyanobacteria by a Phenol-Sulfuric Acid Method. Bio-Protocol 8, 1–13.

Zavřel, T., Schoffman, H., Lukeš, M., Fedorko, J., Keren, N., Červený, J., 2021. Monitoring fitness and productivity in cyanobacteria batch cultures. Algal Res. 56, 1–15.

Zavřel, T., Sinetova, M.A., Búzová, D., Literáková, P., Červený, J., 2015a. Characterization of a model cyanobacterium Synechocystis sp. PCC 6803 autotrophic growth in a flat-panel photobioreactor. Eng. Life Sci. 15, 122–132.

Zavřel, T., Sinetova, M.A., Červený, J., 2015b. Measurement of Chlorophyll a and Carotenoids Concentration in Cyanobacteria. bio-protocol 5, 1–5.

Zavřel, T., Szabó, M., Tamburic, B., Evenhuis, C., Kuzhiumparambil, U., Literáková, P., Larkum, A.W.D., Raven, J.A., Červený, J., Ralph, P.J., 2018c. Effect of carbon limitation on photosynthetic electron transport in Nannochloropsis oculata. J. Photochem. Photobiol. B Biol. 181.